

Large-scale Permo-Triassic back-arc extensions of the Mongol-Okhotsk Ocean

Mingshuai Zhu^{1,2}, John Wakabayashi³, Daniel Pastor-Galán^{4,5}, Fuqin Zhang^{1,2}, Ariuntsetseg Ganbat⁶,
Laicheng Miao^{1,2,†}, Shunhu Yang^{1,2}, and Zeli Wang⁷

¹Key Laboratory of Mineral Resources, Institute of Geology and Geophysics, Chinese Academy of Sciences, Beijing 100029, China

²Institutions of Earth Science, Chinese Academy of Sciences, Beijing 100029, China

³Department of Earth and Environmental Sciences, California State University, Fresno, California 93740, USA

⁴Department of Geodynamics, Universidad de Granada, Campus Fuentenueva, 18071 Granada, Spain

⁵Frontier Research Institute for Interdisciplinary Sciences, Tohoku University, Sendai, Miyagi 980-0845, Japan

⁶Department of Earth Sciences and Laboratory for Space Research, University of Hong Kong, Cyberport 4, Hong Kong, China

⁷Shandong Key Laboratory of Depositional Mineralization and Sedimentary Minerals, Shandong University of Science and Technology, Qingdao 266590, China

ABSTRACT

The Late Paleozoic–Mesozoic Mongol-Okhotsk orogenic belt marks the final aggregation of East Asia. The geodynamics of the Mongol-Okhotsk oceanic plate subduction are still poorly understood due to its curved orogenic architecture, complex kinematics, and the protracted active continent margin that developed during oceanic subduction. Here, we report the discovery of an ophiolite within the southern paleo-active margin of the Mongol-Okhotsk orogenic belt. The ophiolitic slices are composed of serpentinites, metagabbros, and metabasalts, and interleaved with deformed volcaniclastic rocks. Using zircon U-Pb dating, we determined an age of 253 ± 2 Ma for the metagabbro, which suggests that the ophiolite formed during the Late Permian. Geochemical data and geologic relationships indicate that this ophiolite formed in a back-arc setting. The contemporaneous granitic dikes (ca. 255 Ma) intruding the basalts of the ophiolite were likely formed by crustal anatexis during the back-arc extension. Detrital zircon in sandstone associated with the ophiolite shows a prominent peak age of ca. 273 Ma that probably represents the sediments of the back-arc basin. Combining our discovery with the available data from the literature, we suggest that a >5000-km-long back-arc extension belt existed in the southwestern segment of the Mongol-Okhotsk belt, which indicates a probable Western Pacific-

type active margin rather than the previously proposed Andean-type margin that formed during the Permo-Triassic period.

INTRODUCTION

Active continental margins are the places where oceanic crust recycles into the mantle; they serve as the loci of continental crust growth (Stern, 2002; Kearey et al., 2009). There are two endmember types of active continental margins: the Western Pacific type and the Andean type (Uyeda, 1982; Stern, 2002; Li et al., 2012). The Western Pacific-type margins show steep-angled subducting slabs, weak coupling between the slab and overlying plate, and significant extensions in the back-arc and/or island arc regions (Stern, 2010; Zheng et al., 2015). In contrast, the Andean-type margins have gentle-angled subduction slabs with strong coupling between them and overlying plate, and intensive compression of the overriding plate (Ramos and Folguera, 2009; Capaldi et al., 2017). Active margins can evolve from one endmember to the other following the kinematic changes in plate convergence and/or slab rollback rates (Dilek and Sandvol, 2009; Li et al., 2012; Zhang et al., 2017). Identifying significant back-arc extensions in ancient orogens is crucial for discriminating the type of active margin that developed during oceanic subduction at a given time.

The Central Asian Orogenic Belt is possibly the largest preserved accretionary orogen worldwide. It formed through multiple convergence and collision events involving various arcs, terranes, and continental blocks (e.g., Windley et al., 2007; Xiao et al., 2015). The Mongol-

Okhotsk orogenic belt is the youngest segment of the Central Asian Orogenic Belt and extends more than 3000 km to the northeast from central Mongolia to the Uda Gulf in the Okhotsk Sea (Fig. 1; Zorin, 1999; Bussien et al., 2011). The Mongol-Okhotsk orogenic belt has a 180° curved architecture that likely formed during the closure of the Mongol-Okhotsk Ocean (Zorin, 1999; Xiao et al., 2015), which led to the collision of the Siberian Craton and the Amur Block during the Middle Jurassic–Early Cretaceous (Van der Voo et al., 2015; Sorokin et al., 2020; Yi and Meert, 2020). Thus, the Mongol-Okhotsk orogenic belt played a crucial role in the formation and tectonic evolution of East Asia during the Mesozoic (Parfenov et al., 2001; Xu et al., 2013; Tang et al., 2016; Sorokin et al., 2020). Some authors have suggested that the Mongol-Okhotsk Ocean plate subducted northward, beneath the Siberian Craton, and southward, beneath the Amur Block (Metelkin et al., 2007; Donskaya et al., 2013; Tang et al., 2016; Zhao et al., 2017; Li et al., 2017). In most of these proposals, both convergent margins are considered to be Andean-type active margins throughout the long period of subduction (Tomurtogoo et al., 2005; Yarmolyuk et al., 2008; Reichow et al., 2010; Tang et al., 2016; Li et al., 2018). In contrast, Zhu et al. (2016) and Liu et al. (2018) described bimodal volcanic suites and A-type granites (216–207 Ma) in central Mongolia and Northeast China that were interpreted to have formed in back-arc extensional settings at the southern margin of the Mongol-Okhotsk Ocean. These findings prompted us to reevaluate the type and geodynamic evolution of the active margins of the Mongol-Okhotsk Ocean.

[†]Corresponding author: zhumingshuai@mail.iggcas.ac.cn

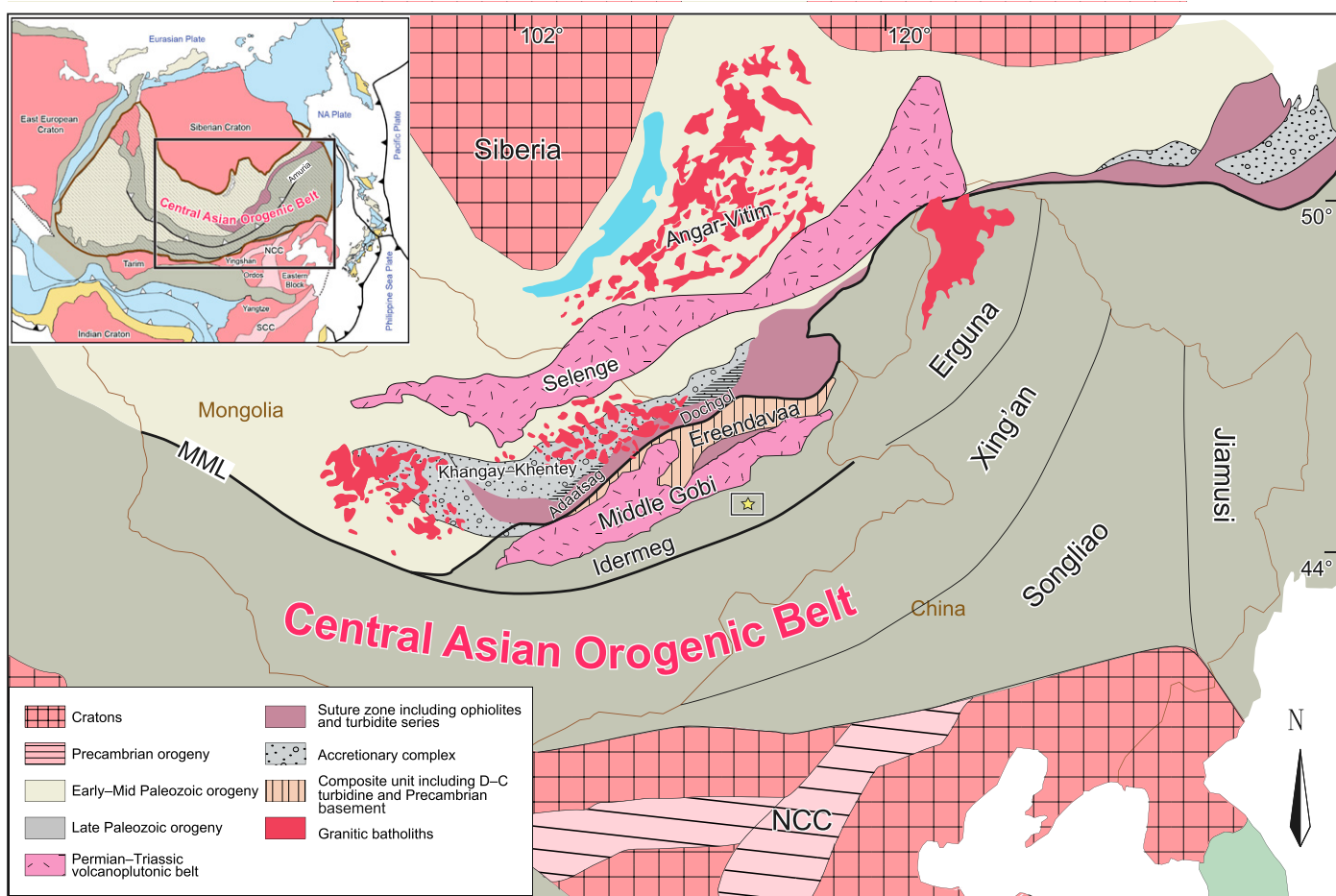


Figure 1. Tectonic map shows the main tectonic units of the Mongol-Okhotsk orogenic belt (modified from Bussien et al., 2011; Xiao et al., 2015). MML—Main Mongolian Lineament; NCC—North China Craton; SCC—South China Craton; NA plate—North American plate; D-C—Devonian-Carboniferous.

In this paper, we present petrographic, geochemical, zircon U-Pb geochronologic, and Hf isotopic data from a newly identified ophiolitic suite, providing insights into the character and tectonic setting of the ophiolite and the geodynamic evolution of the Mongol-Okhotsk orogenic belt. After combining our data with other data sets, we suggest that a >5000-km-long and 200–300-km-wide belt of multi-stage, back-arc extensions formed in the southwestern segment of the Mongol-Okhotsk orogenic belt during the Permo-Triassic.

REGIONAL GEOLOGY AND SAMPLE DESCRIPTION

Mongolia has traditionally been subdivided into an early Paleozoic domain to the north and a late Paleozoic domain to the south, which are separated by the Main Mongolian Lineament (Badarch et al., 2002; Fig. 1). The northern domain is crosscut by the young Mongol-

Okhotsk orogenic belt that formed following the subduction and closure of the Mongol-Okhotsk Ocean (Bussien et al., 2011; Donskaya et al., 2013). In the southwestern segment, the suture zone of the Mongol-Okhotsk orogenic belt was represented by the Adaatsag-Dochgol terrane (Fig. 1), which was composed of chert, metasandstone, metavolcanic rocks, limestone, and ophiolitic mélange (Badarch et al., 2002; Tomurtogoo et al., 2005; Zhu et al., 2018). According to the terrane division of Badarch et al. (2002), the study area is located to the south of the suture zone and is part of the Idermeg terrane; the Middle Gobi magmatic belt lies to the north (Fig. 1).

The Idermeg terrane is possibly part of the Central Mongolia microcontinents (Wilhem et al., 2012), which are thought to correlate with the Tuva-Mongolian microcontinent (Sengör and Natal'in, 1996; Windley et al., 2007). The crystalline basement rocks of the Idermeg terrane mainly consist of gneiss, schist, and

amphibolites, which were overlain by Neoproterozoic to Cambrian conglomerate, sandstone, and limestone (Badarch et al., 2002). The Middle Gobi magmatic belt is probably related to the southward subduction of the Mongol-Okhotsk Ocean plate (Parfenov et al., 2001; Badarch et al., 2002; Tomurtogoo et al., 2005; Zhao et al., 2017). The belt could extend northeast to the Erguna massif in NE China, where abundant Permian-Triassic intrusions and coeval porphyry-type ore deposits were reported (Sun et al., 2013; Xu et al., 2013; Tang et al., 2016; Li et al., 2017). According to Badarch et al. (2002), the basement of this magmatic belt should be the Ereendavaa terrane, which is defined as a cratonic terrane with a Paleoproterozoic basement overlain by Neoproterozoic metasedimentary and volcanic rocks. However, the new results suggest that the ascribed Precambrian gneiss, amphibolite, and schist of the Ereendavaa terrane mainly formed during the early-middle Paleozoic (512–419 Ma). They are proposed to

have resulted from the evolution of the Kherlen Ocean evidenced by the Kherlen ophiolite (ca. 566–510 Ma; Miao et al., 2016; Narantsetseg et al., 2019). The final closure of the Kherlen Ocean is proposed to have occurred during the Silurian, leading to the amalgamation of the Ereendavaa and Idermeg continental terranes (Miao et al., 2016; Narantsetseg et al., 2019); together, they constitute the southern continental margin of the Mongol-Okhotsk Ocean.

The newly discovered ophiolite is located ~30 km southwest of the city of Monhhan, Mongolia. The Monhhan ophiolite crops out over an area of $2 \text{ km} \times 3 \text{ km}$ as tectonic slices of up to 0.5 km in length along-strike and 0.1 km in structural thickness and is interleaved with the volcano-sedimentary Khukh Ovoot Formation (Fig. 2). The ophiolitic slices are composed of serpentinites, metagabbros and metabasalts

(Fig. 3). The Khukh Ovoot Formation consists of limestone, metasiltstone, quartzite, and metasandstone intruded by Triassic–Jurassic granites and has experienced greenschist-facies metamorphism and varying degrees of deformation (Fig. 3F). This formation was assigned to the Precambrian (Jamyandorj et al., 1990), but actually no isotopic age has ever been reported. The harzburgite experienced strong serpentinitization (Figs. 4A and 4B). The metagabbro shows a poikilitic texture and is composed of pyroxene (~15%), amphibole (~35%), and plagioclase (~50%) (Figs. 4C and 4D). The basalt experienced variable hydrothermal alteration, and most of the pyroxenes have been altered to amphibole (Figs. 4E and 4F). Locally, granite dikes of up to 20 cm wide occur within the basaltic lavas and show an exsolution texture (Figs. 4G and 4H).

ANALYTICAL METHODS

Geochemistry

Whole-rock major and trace element compositions were determined at the Wuhan Sample Solution Analytical Technology Co., Ltd., Wuhan, China, by X-ray fluorescence (XRF) and inductively coupled plasma–mass spectrometry (ICP-MS). The precision of the XRF analyses is within $\pm 2\%$ for the oxides greater than 0.5 wt% and within $\pm 5\%$ for the oxides greater than 0.1 wt%. Analytical results for U.S. Geological Survey standards indicated that the data are accurate within $\pm 5\%$ for the trace elements.

Zircon U-Pb Geochronology

Zircon crystals were extracted from samples by conventional heavy liquid and magnetic separation techniques and were then hand-picked under a binocular microscope. The zircon grains were mounted in epoxy and polished so that the zircon interiors were exposed. Optical photographs and cathodoluminescence (CL) images were prepared to study the internal textures and origins of the zircons and to select optimal sites for analysis.

Zircon U-Pb dating by laser ablation–inductively coupled plasma–mass spectrometry (LA-ICP-MS) was conducted at Key Laboratory of Regional Geology and Mineralization, Hebei GEO University, Shijiazhuang, China. For the present work, laser spot size was set to $29 \mu\text{m}$ for most analyses, laser energy density at 3 J/cm^2 , and the repetition rate at 8 Hz. Calibrations for the zircon analyses were carried out using NIST 610 glass as an external standard and Si as the internal standard. Zircon 91500 was used as primary reference material, whereas zircon GJ-1 (609 Ma; Jackson et al., 2004) and Plešovice (337 Ma; Sláma et al., 2008) were used to check accuracy. Isotopic ratios and element concentrations of zircons were calculated using Iolite software (Paton et al., 2010). Concordia ages and diagrams were obtained using ISOPLOT 3.0 (Ludwig, 2003). The analyses for standards GJ-1 and Plešovice yielded weighted mean $^{206}\text{Pb}/^{238}\text{U}$ ages of $606 \pm 5 \text{ Ma}$ and $336.5 \pm 2 \text{ Ma}$, respectively, which are in agreement with their respective reference values.

Zircon Hf Analysis

In situ zircon Lu-Hf isotopes were carried out by the inductively coupled plasma–multicollector–mass spectrometer (ICP-MC-MS) at the Createch Testing Technology Co., Ltd., in Beijing, China. The laser ablation beam spot was $40 \mu\text{m}$

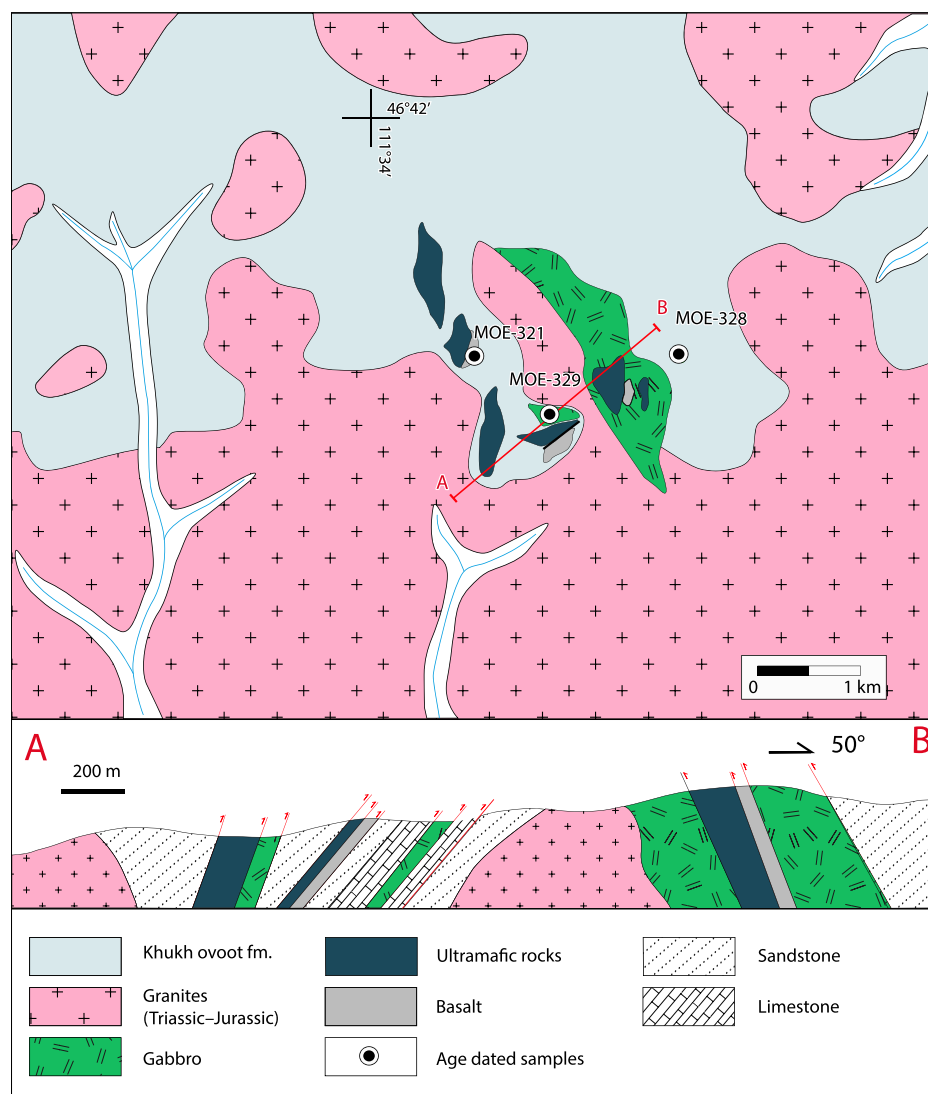


Figure 2. Geological map and cross section of the Monhhan ophiolite are shown.

in diameter, and the analyzed pulse frequency of the laser beam was 8 Hz. Detailed analytical procedures are described in Wu et al. (2006). In the calculation of the $\epsilon\text{Hf(t)}$ values, the $^{176}\text{Hf}/^{177}\text{Hf}$ and $^{176}\text{Lu}/^{177}\text{Hf}$ ratios of present-day chondrite and the depleted mantle were (0.0332, 0.282772) and (0.0384, 0.28325), respectively (Blichert-Toft and Albarède, 1997; Griffin et al., 2000). The two-stage Hf model ages (T_{DM2}) were calculated assuming a value of $^{176}\text{Lu}/^{177}\text{Hf} = 0.015$ for the average continental crust (Griffin et al., 2004). The $^{176}\text{Hf}/^{177}\text{Hf}$ value of the standard zircon Plešovice tested in this experiment was 0.282480 ± 0.000016 (2σ), which is consistent with the value of the predecessor (Sláma et al., 2008) and within the error range.

RESULTS

Geochemistry

Typical whole-rock geochemistry of different lithologies from the ophiolite is given in Supplementary Material Table S1¹. The harzburgites are characterized by low SiO_2 (39.98 wt% and 40.59 wt%) and high MgO (38.95 wt% and 39.55 wt%), with $\text{Mg}^{\#}$ [= molar $\text{Mg}/(\text{Mg} + \text{Fe}^{2+})$] of 0.92. The gabbros have SiO_2 (55.17–58.41 wt%), MgO (1.32–2.57 wt%), Na_2O (3.46–5.58 wt%), and TiO_2 (0.64–1.32 wt%). They show light rare earth element (LREE) enrichment, Nb-Ta and Ti negative anomalies, and slightly elevated large-ion lithophile elements (LILEs) (Figs. 5A and 5B). The basalts have SiO_2 contents of 46.81–51.13 wt%, and Al_2O_3 , MgO , Na_2O , K_2O , and TiO_2 contents of 14.30–18.58 wt%, 4.49–7.61 wt%, 2.40–4.43 wt%, 1.13–1.89 wt%, and 1.51–2.85 wt%, respectively. They exhibit high LREE/HREE ratios [$(\text{La/Yb})_N$ of 2.88–14.0] and enrichment in LILEs and moderate negative anomalies in Nb, Ta, and Ti (Figs. 5C and 5D). The granite dikes intruding the basalts have high SiO_2 (77.14–77.72 wt%), Na_2O (3.33–3.36 wt%), and K_2O (4.93–4.94 wt%) contents, but low MgO (0.10–0.11 wt%), CaO (0.39–0.40 wt%), and $\text{Fe}_2\text{O}_3^{\text{T}}$ (0.59–0.60 wt%) contents.

¹Supplemental Material. Figure S1: Discrimination diagrams for the granite dikes in the Monhhan ophiolite. Table S1: Major and trace element compositions of the Monhhan ophiolite and intruding granite. Table S2: LA-ICP-MS zircon U-Pb analytical data for the gabbro, intruding granite, and associated sandstone in the Monhhan ophiolite. Table S3: Lu-Hf data for zircons from the gabbro and intruding granite in the Monhhan ophiolite. Please visit <https://doi.org/10.1130/GSAB.S.21448209> to access the supplemental material, and contact editing@geosociety.org with any questions.

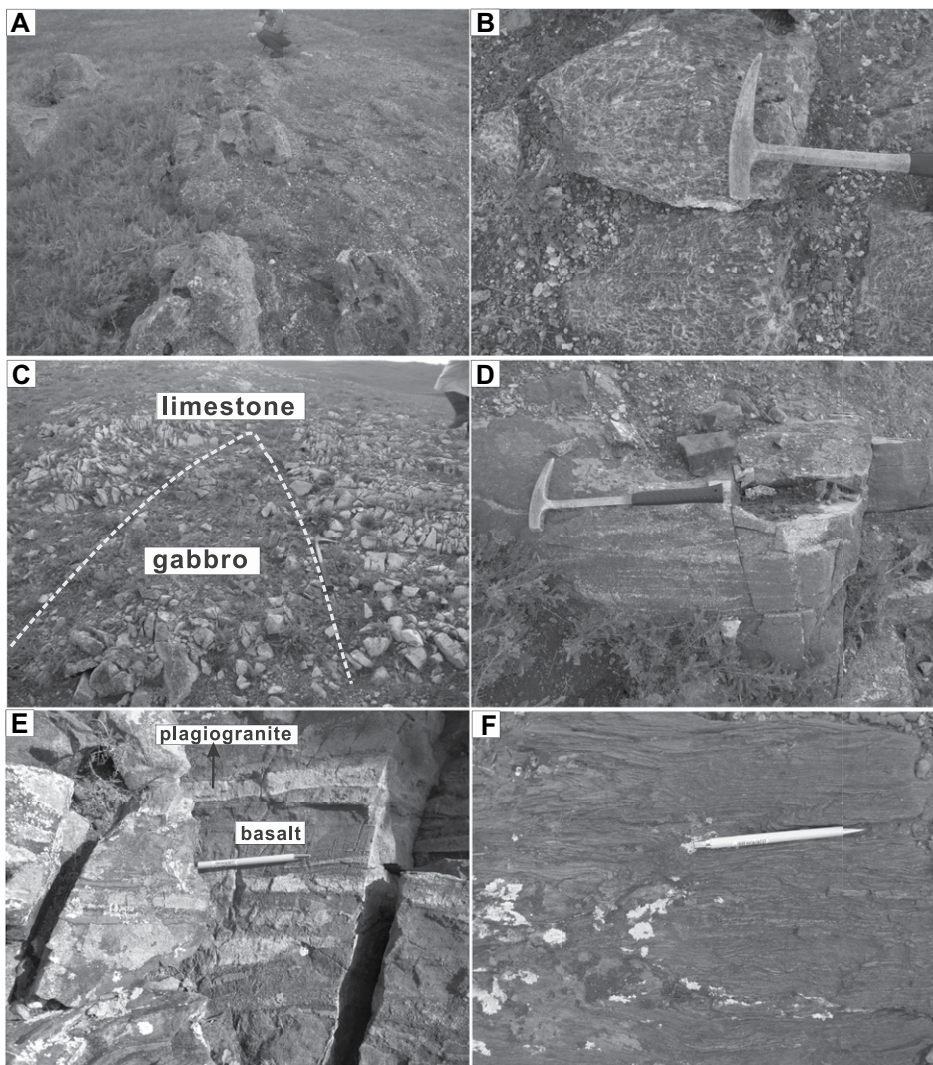


Figure 3. Field photographs of the Monhhan ophiolite and associated Khukh Ovoot Formation are shown. (A) Serpentized ultramafic rocks. **(B)** Serpentized harzburgite shows deformation fabric and orthopyroxene pseudomorph. **(C)** Metagabbro tectonic slice of the Monhhan ophiolite in tectonic contact with the limestone of the Khukh Ovoot Formation. **(D)** Layered gabbro of the Monhhan ophiolite. **(E)** Granite dikes intruded the basaltic rocks of Monhhan. **(F)** Deformed sandstone of the Khukh Ovoot Formation.

Zircon U-Pb Geochronology and Hf Isotope Composition

One gabbro sample from the ophiolite, one sample from the granite dike, and one sandstone sample from the Khukh Ovoot Formation were selected for LA-ICP-MS U-Pb zircon dating and Hf isotope analysis (analytical data in Tables S2 and S3; see footnote 1). Zircons from the gabbro sample MOE-325 are euhedral to subhedral prisms that are 100–300 μm long and show oscillatory zoning (Fig. 6A). The measured U and Th concentrations vary from 173 ppm to 643 ppm and from 110 ppm to 565 ppm, respectively, with Th/U ratios

between 0.22 and 1.22, which indicates an origin of igneous zircon (e.g., Rubatto, 2002). Twenty-five analyses yielded a weighted mean $^{206}\text{Pb}/^{238}\text{U}$ age of 253 ± 2 Ma (MSWD = 1.9; Fig. 6B), which is considered to be the time of zircon crystallization. Eleven spots analyses yielded older ages of ca. 444–597 Ma, which are interpreted to represent zircon inheritance. The zircons with young ages (249–259 Ma) have positive $\epsilon\text{Hf(t)}$ values (+4.28 to +7.28), and the inherited zircons have negative $\epsilon\text{Hf(t)}$ values (−4.72 to −0.85; Fig. 6C).

Zircons from sample MOE-321, which is composed of granite that intrudes the basalts of the Monhhan ophiolite, are 80–200 μm in size.

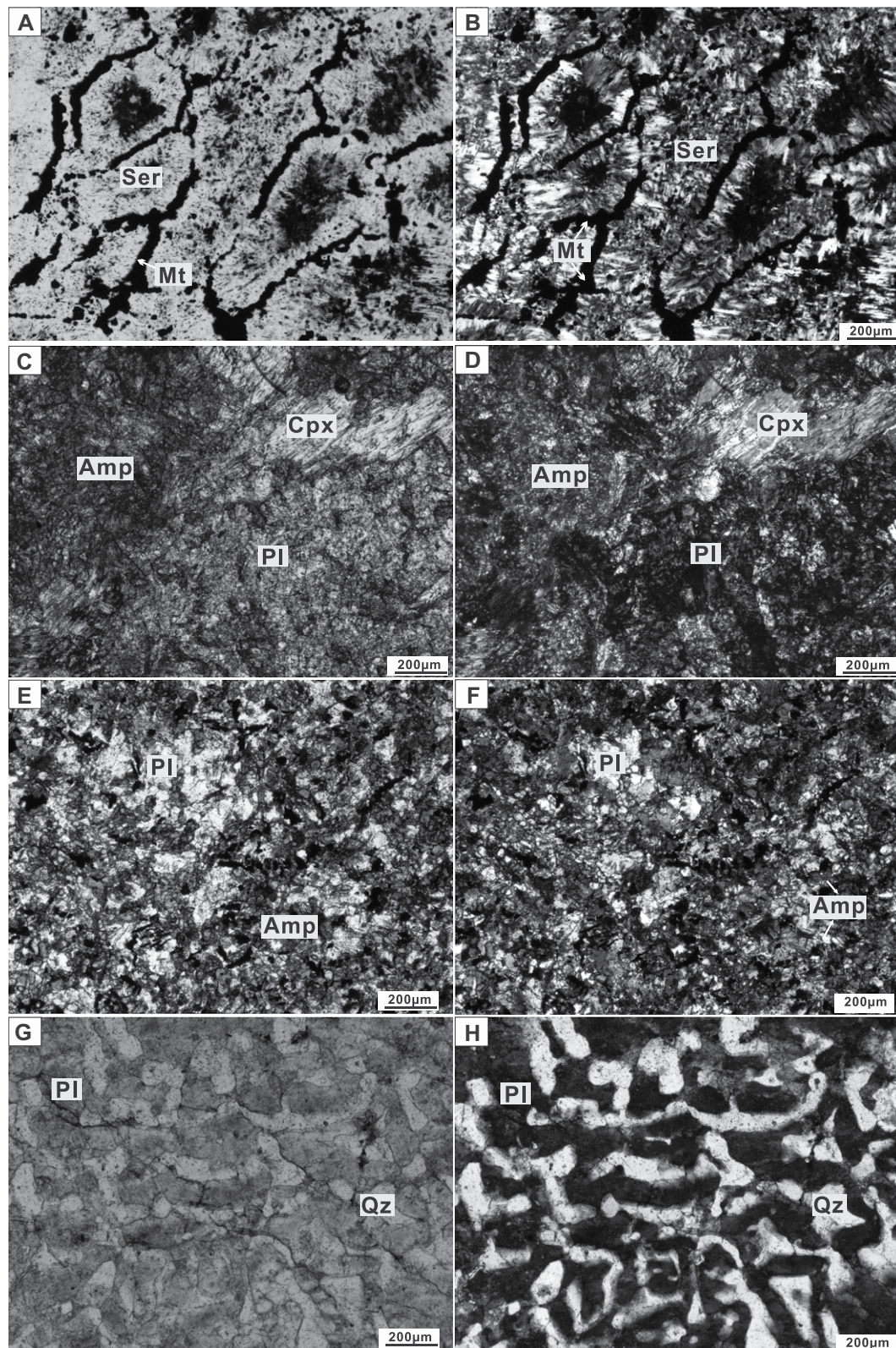


Figure 4. Photomicrographs of different rocks from the Monhhan ophiolite are shown. (A, B) Medium- to coarse-grained harzburgite shows strong serpentinization. (C, D) The metagabbro from the Monhhan ophiolite shows a poikilitic texture. (E, F) Basaltic rocks show alteration. (G, H) Granite shows an exsolution texture. Ser—serpentinite; Mt—magnetite; Cpx—clinopyroxene; Pl—plagioclase; Amp—amphibole; Qz—quartz.

Most zircons show typical oscillatory zoning (Fig. 6A) with Th/U ratios ranging from 0.66 to 1.43, which indicates a magmatic origin for the zircons. Twenty-one analyses yielded

a concordia weighted mean $^{206}\text{Pb}/^{238}\text{U}$ age of 255 ± 2 Ma (MSWD = 2.3; Fig. 6D), which is interpreted to record the time of zircon crystallization. Eighteen spot analyses yielded high

initial $^{176}\text{Hf}/^{177}\text{Hf}$ ratios and positive $\varepsilon_{\text{Hf}}(t)$ values (+2.81 to +10.59), and model ages of $T_{\text{DM}2}$ (599–1094 Ma) similar to those of the young zircons of the gabbro (Fig. 6C).

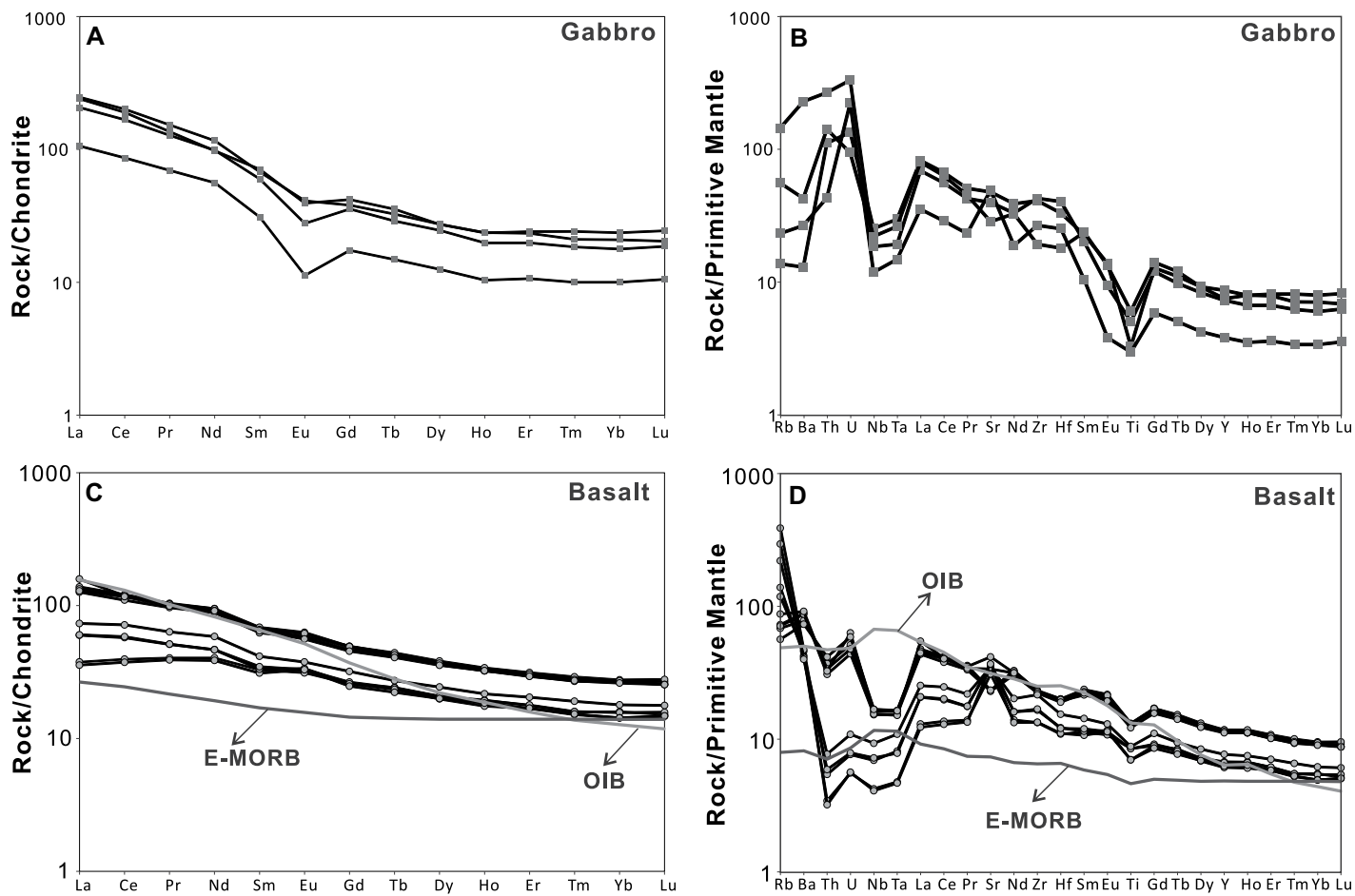


Figure 5. Chondrite-normalized rare earth element patterns and primitive mantle-normalized diagrams for the (A, B) gabbro and (C, D) basalt of the Monhhan ophiolite. Normalizing values for both chondrite and primitive mantle are from Sun and McDonough (1989).

Zircons from sandstone sample MOE-338, collected from the Khukh Ovoot Formation, are euhedral to subhedral and 50–150 μm long. Most zircons display oscillatory zoning (Fig. 6A). A total of 45 zircon grains were analyzed and yielded apparent ages ranging from ca. 234–449 Ma, with the most evident age peak at ca. 273 Ma (Figs. 6E and 6F).

DISCUSSION

Age and Tectonic Setting of the Monhhan Ophiolite

This study was the first to identify ophiolite within the southern active paleomargin of the Mongol-Okhotsk Ocean rather than in the Mongol-Okhotsk suture zone. The gabbro from the Monhhan ophiolite yielded a zircon U-Pb age of 253 ± 2 Ma, which suggests that the ophiolite formed during the Late Permian. The inherited zircon grains (444–597 Ma) from the gabbro sample were possibly derived from the early Paleozoic orogeny related to the evolution of

the Kherlen Ocean between the Ereendavaa and Idermeg terrane (e.g., Miao et al., 2016).

Mantle-derived magmas are often contaminated by continental crust during magma ascent. However, no correlation of Nb/La and Th/La with SiO₂, the very low Th/Ce (0.01–0.05), and Th/La (0.03–0.12) ratios rule out significant crustal contamination for the basalts of the Monhhan ophiolite, because continental crust has relatively high Th/Ce (~0.15; Taylor and McLennan, 1995) and Th/La (~0.30; Plank, 2005). Similarly, the Th/Ta ratios of the basalts range from 1.38 to 5.28, which are close to the primitive mantle value (Th/Ta = 2.3) but different from the continental crust value (Th/Ta = 10; Sun and McDonough, 1989) and also indicate insignificant crustal contamination. The basalts show LREE and LILE enrichment and depletion of Nb-Ta-Ti, which, combined with the positive $\epsilon_{\text{Hf}}(t)$ values of the gabbro, indicates that they may have been derived from a depleted mantle source metasomatized by subduction-derived components (e.g., Stern, 2002). This hypothesis is further supported by most samples fall-

ing above the mid-oceanic-ridge basalt–oceanic island basalt (MORB-OIB) array in the Th/Yb versus Nb/Yb diagram (Fig. 7A; Pearce, 2008), which suggests that the Monhhan mafic-ultramafic rocks represent an SSZ-type ophiolite. Such ophiolite can form in back-arc and forearc basin settings (e.g., Dilek and Furnes, 2011). The Monhhan basaltic rocks have enriched LREEs, unlike the forearc basin basalts with depleted LREEs (Dilek and Furnes, 2011). Mafic magma in back-arc settings could show a wide range of compositions: arc-like basalt, MORB, and back-arc basin basalts (BABBs; e.g., Gribble et al., 1998; Pearce, 2008). All of the Monhhan basaltic rocks plot in the BABB fields on the Th/Yb versus Nb/Yb diagram (Pearce, 2008; Fig. 7A) and Hf/3-Yb-Nb/16 diagram (Wood, 1980; Fig. 7B). On the Nb_N versus Th_N diagram (Saccani, 2015), the basalt samples plot in the BABB field and continental margin volcanic-arc field (Fig. 7C). On the Nb/Y versus Zr/Y diagram (Condie, 2005), the basalt samples fall in the arc field (Fig. 7D). Hence, we infer that the Monhhan ophiolite formed in a back-arc tectonic

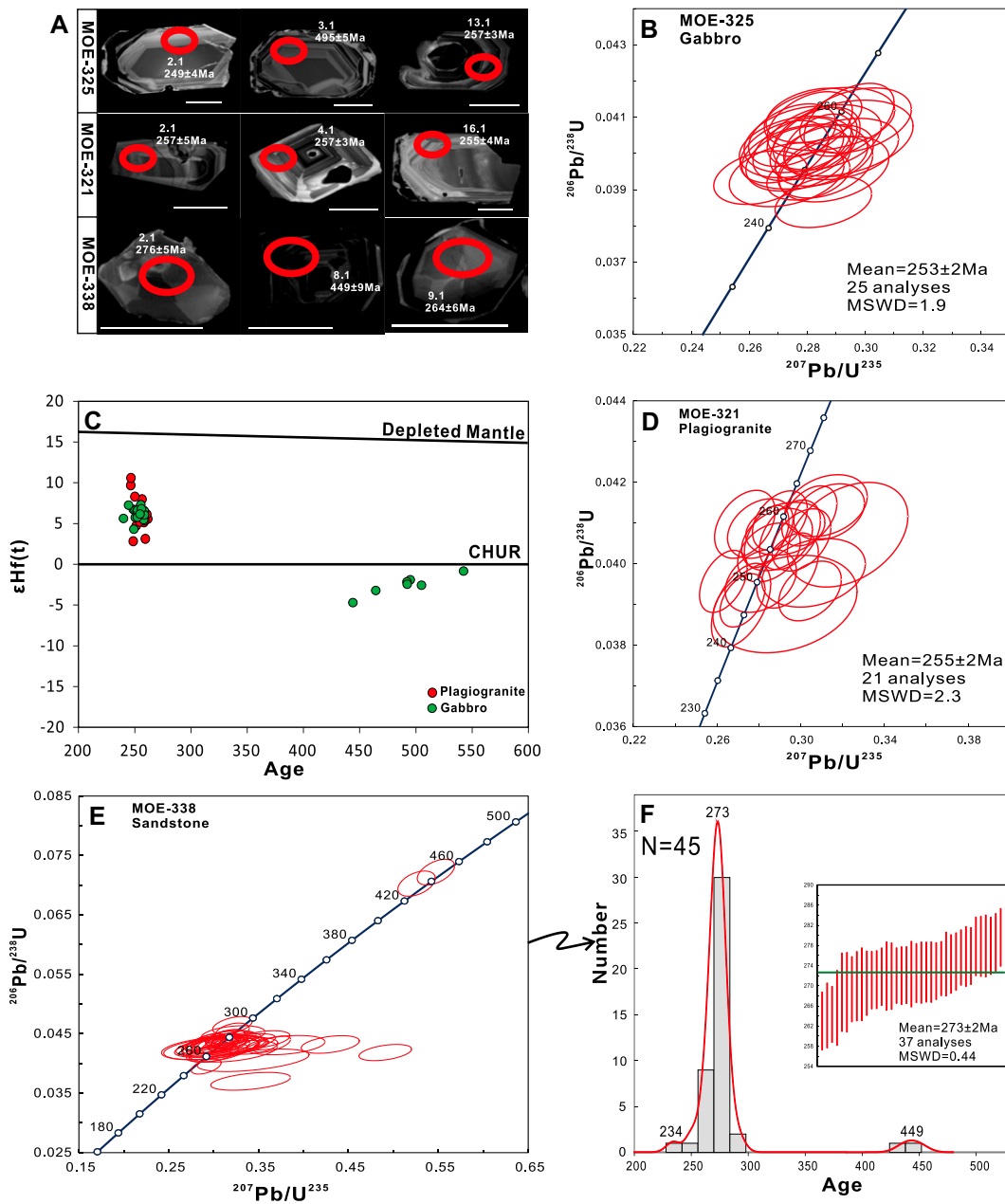


Figure 6. Zircon cathodoluminescence (CL) images, $\epsilon\text{Hf}(t)$, and U-Pb concordia diagrams of the Monhan ophiolite are shown. (A) Representative CL images of zircons from this study. Red circles represent sites of analytical spots, and the numbers around the circles are the spot numbers and ages (with 2σ error). The scale bar is 50 μm . (B) U-Pb concordia diagram of the gabbro. (C) Zircon U-Pb age versus $\epsilon\text{Hf}(t)$ diagram for the gabbro and granite. (D) U-Pb concordia diagram of the plagiogranite. (E, F) Detrital zircon U-Pb concordia and relative probability diagrams for the sandstone of the Khukh Ovoot Formation. CHUR—Chondritic uniform reservoir; MSWD—mean square of weighted deviates.

setting. The basalts from different tectonic slices show different geochemical characteristics (Figs. 5C and 5D), which indicates that they probably document different stages of back-arc evolution as the subduction continues (Saunders and Tarney, 1984).

The granite dikes show very high K_2O and low CaO contents distinct from the mafic rocks of the ophiolite, which indicates that they neither formed through extreme fractional crystallization of a mantle-derived melt nor partial melting of hydrated mafic crust (e.g., Koepke et al., 2007; Brophy, 2009; Furnes and Dilek, 2017). They have A/CNK values ranging from 1.06 to 1.07, which demonstrate a peraluminous feature

(Fig. S1A; see footnote 1). The positive correlation between P_2O_5 and SiO_2 (Fig. S1B) indicates that they are S-type granites (Dan et al., 2014), as evidenced by how they plot in the ACF diagram (Fig. S1C). S-type granites are usually generated by partial melting of metasediments in the middle and lower crust (Gao et al., 2017; Hopkinson et al., 2017). In the Rb versus ($\text{Y} + \text{Nb}$) discrimination diagram (Pearce et al., 1984), the granitic samples fall into the volcanic arc field (Fig. S1D). Considering their ages are similar to those of the ophiolite, we suggest that the granites were probably formed by partial melting of crust as a result of magma underplating during back-arc extension, similar to the S-type

granites in circum-Pacific orogens (Collins and Richards, 2008).

The youngest zircon age of the sandstone indicates that the Khukh Ovoot Formation has a maximum depositional age of Late Triassic rather than Precambrian as previously thought (Figs. 6E and 6F). During this period, a number of depressions and grabens filled with bimodal volcanic suites, A-type granites, and clastic sedimentary rocks developed in this region (Yarmolyuk et al., 2002; Dostal et al., 2015; Zhu et al., 2016). Geochemical evidence indicates that the bimodal volcanic rocks and the coeval A-type granites (213–207 Ma) were generated in an intra-continental back-arc basin

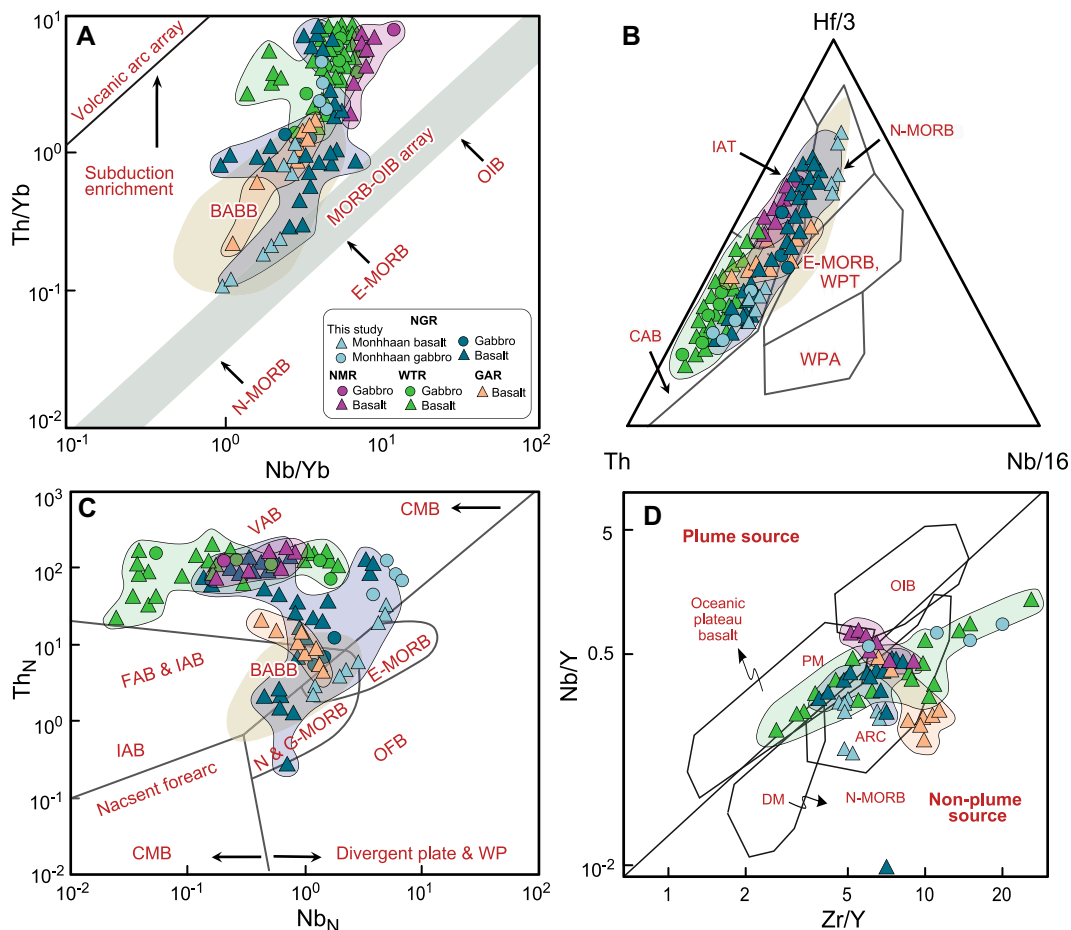


Figure 7. Geochemical plots of mafic rocks from the Monhhan ophiolite as well as the Permian–Triassic rifts are shown. (A) Nb/Yb versus Th/Yb discrimination diagram (Pearce, 2008). (B) Hf/3–Th–Nb/16 diagram (Wood, 1980). (C) Nb_N versus Th_N diagram (Saccani, 2015). (D) Zr/Y versus Nb/Y diagram (Condie, 2005). Normalizing values are from Sun and McDonough (1989). Data for the Okinawa back-arc basin basalts (BABBs) in panel A are from Shinjo et al. (1999). The field for the BABB in panel B is from plots of 2340 BABB samples by Yang et al. (2016). Western Trans-Baikalian rift data are from Berzina et al. (2009), Jahn et al. (2009), Donskaya et al. (2012), and Yarmolyuk et al. (2014); Gobi-Altai rift (GAR) data are from Kozlovsky et al. (2005) and Yarmolyuk et al. (2014); northern Mongolian rift (NMR) data are from Yarmolyuk et al. (2014, 2016); North Gobi Rift (NGR) data are from Yarmolyuk et al. (2014) and Zhu et al. (2016). ARC—arc-related

basalts; CAB—calc-alkaline basalt; CMB—convergent plate settings; DM—depleted mantle; FAB—forearc basalt; IAB—island-arc basalt; IAT—island-arc tholeiites; E-MORB—enriched mid-oceanic-ridge basalt; G-MORB—garnet-influenced mid-oceanic-ridge basalt; MORB-OIB—mid-oceanic-ridge basalt–oceanic-island basalt; N-MORB—normal mid-oceanic-ridge basalt; OFB—oceanic-floor basalt; PM—primitive mantle; WPA—within-plate alkali basalt; WPT—within-plate tholeiites; VAB—volcanic-arc basalt; WP—within-plate..

(Zhu et al., 2016). Most importantly, the Late Permian Monhhan ophiolite and associated Khukh Ovoot Formation are located at the back of the Middle Gobi Permo-Triassic arc-related magmatic front (Fig. 1). Thus, we argue that the Monhhan ophiolite and the Khukh Ovoot Formation represent a relict back-arc basin that developed at the southern active margin of the Mongol-Okhotsk Ocean.

Andean-Type versus Western Pacific-Type Active Margin

Southward subduction of the Mongol-Okhotsk Ocean plate is represented by subduction-related Permian–Jurassic magmatic rocks in the Amur Block (e.g., Tang et al., 2016; Zhao et al., 2017). Northward subduction of the Mongol-Okhotsk Ocean plate was documented by the middle Carboniferous to Triassic Selenge arc and the Angar-Vitim granitoids in Transbaikalia (Fig. 1;

Mazukabzov et al., 2010; Donskaya et al., 2013). Andean-type active margins were proposed to have developed throughout the entire period of Mongol-Okhotsk Ocean plate subduction (Tomurtogoo et al., 2005; Reichow et al., 2010; Tang et al., 2016; Li et al., 2018). However, the newly defined Monhhan Late Permian back-arc ophiolite and coeval Middle Gobi magmatic arc suggest that an arc–back-arc system developed in the southern margin of the Mongol-Okhotsk Ocean. Moreover, as shown by the presence of inherited zircons in the ophiolite, the back-arc basin would have probably opened in the continental domain, similar to the Okinawa trough from a 2-D perspective (Shinjo et al., 1999). These results indicate that a Western Pacific-type active margin probably formed in some regions during the southward subduction of the Mongol-Okhotsk Ocean.

The most prominent records of back-arc extensions of the Mongol-Okhotsk Ocean

show the development of several parallel rift zones filled with bimodal volcanic suite and A-type alkaline granite (Yarmolyuk et al., 2013; Li et al., 2022). In the southern margin of the Mongol-Okhotsk Ocean, the NE-trending North Gobi rift consists of a number of depressions and grabens filled by the Late Permian–Late Triassic clastic sedimentary rocks, which are intercalated with and overlain by bimodal volcanic suites (Yarmolyuk et al., 2002; Dostal et al., 2015). The geochronological data demonstrate that the bimodal volcanic rocks and A-type granites in the rift zone formed during the Late Triassic (221–207 Ma; Yarmolyuk et al., 2002; Zhu et al., 2016). This rift zone probably extended to the Erguna-Xing'an massif in NE China, where the ca. 225 Ma bimodal igneous rock association and ca. 216 Ma A-type granite occur (Tang et al., 2016; Liu et al., 2018). The Gobi-Altai rift zone extends for more than 800 km along the northern face of the Gobi Altai Range and

comprises a linear array of grabens filled with a bimodal volcanic suite and related alkaline granites (Yarmolyuk et al., 2013, 2014). The flora and fauna imprints found in the sedimentary rocks and the ages of the igneous rocks (293–269 Ma) suggest that the Gobi-Altai rift zone formed during the Early–Late Permian (Izokh et al., 2011; Yarmolyuk et al., 2014; Kozlovsky et al., 2015). Previous studies suggest that the formation of this Permian–Triassic, rift-related magmatism was related to the activity of mantle plumes, and the northeastward migration of magmatism resulted from the movement of the Siberian continent and Central Asian Orogenic Belt above the mantle hotspot (Kuzmin et al., 2010; Yarmolyuk et al., 2014). However, the distance between the Gobi-Altai rift and the coeval Tarim plume (>1600 km) is too great even for far-field effects of the mantle plume to have played a role in its formation (Kozlovsky et al., 2015). In addition, the mafic rocks in these rifts are characterized by negative Nb, Ta, and Ti anomalies and enrichment in LILEs, which indicates that they are influenced by subduction processes (Zhu et al., 2016; Tang et al., 2016). This is evidenced by the fact that most of the mafic rocks plot in the volcanic arc fields in various tectonic discrimination diagrams (Fig. 7). A-type felsic magmas could occur in various extensional tectonic regimes, involving within-plate, post-collisional, and back-arc extensional settings (e.g., Eby, 1990, 1992), and can be subdivided into A_1 - and A_2 -type granites (Eby, 1992). The A_1 -type derives from sources such as oceanic-island basalts and were emplaced in anorogenic settings (hotspots, plumes, or continental rift zones), whereas the A_2 type possess arc-like geochemical features and were likely emplaced in post-collisional or back-arc settings. The A-type granitoids and felsic volcanics of the Permian–Triassic rifts within the southern margin of the Mongol-Okhotsk Ocean plot in the A_2 field on the Y–Nb–Ce diagram (Fig. 8). Late Triassic subduction records (e.g., Zhu et al., 2016; Li et al., 2018; Ganbat et al., 2021) and paleomagnetic data (Cogné et al., 2005; Ren et al., 2018; Yi and meert, 2020) constrain the final closure of the Mongol-Okhotsk Ocean to the Jurassic–Cretaceous, which indicates that these A_2 -type granites probably documented back-arc extensional settings rather than post-collisional extensional regimes. Permian S-type granites (273–254 Ma) have been identified along the southern margin of the Middle Gobi magmatic arc belt and are thought to have generated in an active margin related to the southward subduction of the Mongol-Okhotsk Ocean (Zhao et al., 2017). In subduction settings, the origin of S-type granites has been attributed to back-arc extensions associated with slab retreat

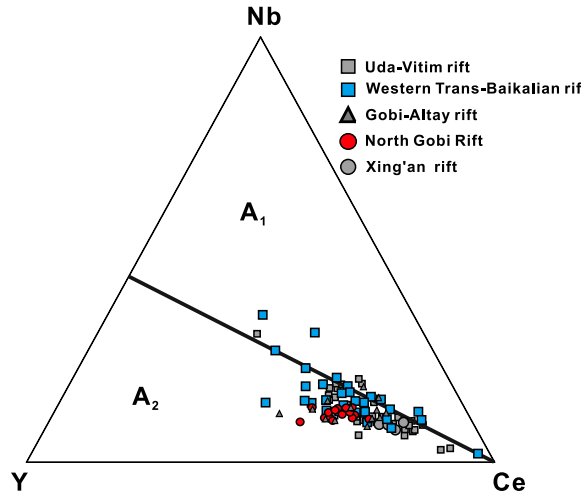


Figure 8. Y–Nb–Ce diagram for the A-type granitoids and felsic volcanics in the Permian–Triassic rifts within the active margins of the Mongol-Okhotsk Ocean is shown. Uda-Vitim rift and Western Trans-Baikalian rift data are from Yarmolyuk et al. (2001), Litvinovsky et al. (2002), Vorontsov et al. (2007), Jahn et al. (2009), and Reichow et al. (2010); Gobi-Altai rift data are from Kozlovsky et al. (2015); North Gobi rift data are from Zhu et al. (2016); Xing'an Triassic rift data are from Liu et al. (2018). A_1 and A_2 denote the respective subgroup granites of Eby (1992).

(Collins and Richards, 2008; Xu et al., 2021) or anatexis of the forearc accretionary complex (Lytwyn et al., 2000; Cole and Stewart, 2009). Apparently, these S-type granites occur far from the forearc belt located along the northern margin of the Ereendavaa terrane (Kelty et al., 2008; Bussien et al., 2011), which indicates that the S-type granites result from back-arc extensions of the Mongol-Okhotsk Ocean. Thus, together the back-arc ophiolite, bimodal volcanic suites, A_2 -type granites, and S-type granites outline a Permian–Triassic back-arc belt with multistage extensions within the southern active margin of the Mongol-Okhotsk Ocean. The forearc belt along the northern margin of the Ereendavaa terrane near the suture zone, the Permian–Triassic Middle Gobi magmatic arc belt in the middle, and the back-arc extension belt in the south constitute a trench–arc–backarc basin system that is typical of the Western Pacific-type active margin.

In the northern margin of the Mongol-Okhotsk Ocean, three rift zones have been delineated, namely the Northern Mongolian, Western Trans-Baikalian, and Uda-Vitim (Fig. 9). The Northern Mongolian rift zone has been traced for ca. 600 km along the northern boundary of the Khangay batholith and includes alkaline granite intrusions in the eastern segment and a few depressions in the western segment (Vorontsov et al., 2007; Yarmolyuk et al., 2013). The largest Orkhon depression is filled with conglomerates, sandstone, and siltstones in the lower part, and basaltic trachyandesites, basalts, trachyandesites, and trachytes in the upper part (Vorontsov et al., 2007). Some occurrences of pillow lavas with hyaloclastic cement in the rift indicate submarine eruptions (Vorontsov et al., 2007). Paleobotanical and geochronological data suggest that the rift was generated during the

Early–Late Permian (249–269 Ma) (Yarmolyuk et al., 2013, 2014). The Western Trans-Baikalian rift zone stretches for more than 1000 km and is composed of bimodal basalt-comendite and basalt-pantellerite volcanic complexes and alkaline granite intrusions (Kovalenko et al., 2003; Vorontsov et al., 2007). The geochronological data suggest these magmatic rocks were formed at 230–210 Ma (e.g., Jahn et al., 2009; Yarmolyuk et al., 2014). The Uda-Vitim rift zone hosts numerous gabbro-monzonite, alkaline granite, granosyenite, syenite massifs, and a bimodal volcanic complex with an age range of 298–275 Ma (e.g., Jahn et al., 2009; Reichow et al., 2010).

There are three main hypotheses to explain these extension features in the northern margin of the Mongol-Okhotsk Ocean. The first hypothesis assumes that they are the result of mantle plumes (Kuzmin et al., 2010; Yarmolyuk et al., 2014). However, the long duration of the Permo-Triassic magmatism is in strong contrast to the short pulses (ca. 1–5 Ma) of magmatism related to the mantle plume (Bryan and Ernst, 2008). The second hypothesis proposes that the Early Permian and Late Triassic alkaline magmatic complexes in the Uda-Vitim and Western Trans-Baikalian belts were linked to post-collisional continental rifting of the Central Asian Orogenic Belt or the Mongol-Okhotsk orogenetic belt (e.g., Jahn et al., 2009; Reichow et al., 2010). However, collisional event in this part of the Central Asian Orogenic Belt occurred during the Ordovician resulting from the Precambrian microcontinents and Neoproterozoic to early Paleozoic subduction-accretionary complex being accreted to the Siberian Craton (Windley et al., 2007; Gladkochub et al., 2008; Rytsev et al., 2009). Thus, the Permian–Triassic alkaline magmatic complexes are not likely related to the

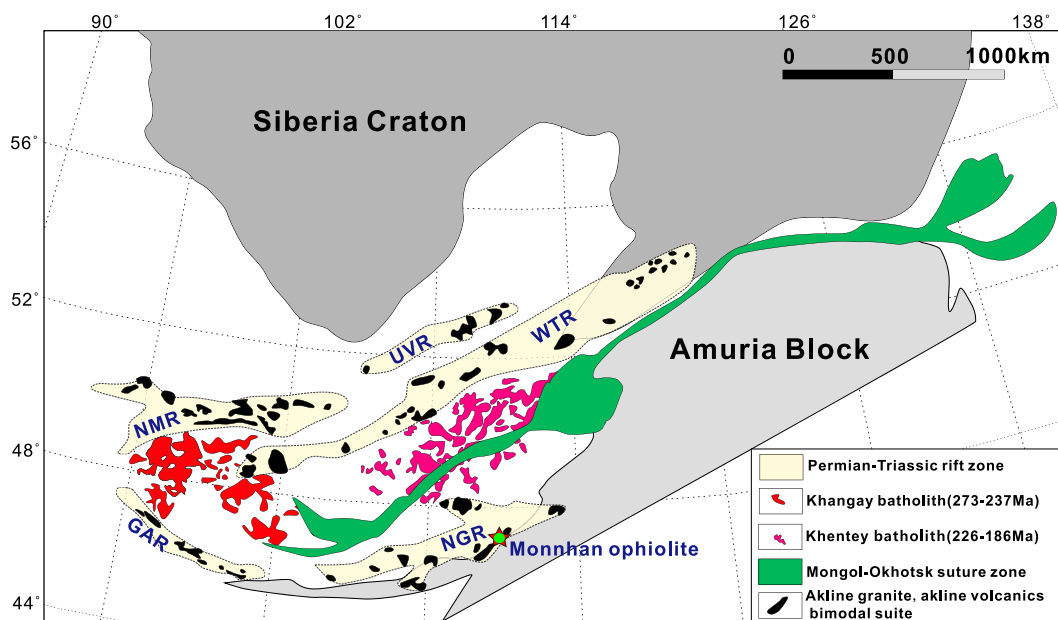


Figure 9. The distribution of Permian-Triassic back-arc extension regimes in the southwestern segment of the Mongol-Okhotsk Ocean is shown (modified from Yarmolyuk et al., 2014). NGR—North Gobi rift; GAR—Gobi-Altai rift; NMR—Northern Mongolian rift; UVR—Uda-Vitim rift; WTR—Western Trans-Baikalian rift.

evolution of the Central Asian Orogenic Belt. As mentioned above, the final closure time of the Mongol-Okhotsk Ocean is estimated to have occurred during the Jurassic-Cretaceous, which indicates that the Permian-Triassic alkaline magmatic complexes did not likely form during the post-collisional setting of the Mongol-Okhotsk orogenic belt. The third hypothesis suggests that the alkaline granitoids and bimodal magmatism formed in a hinterland extensional setting above the broken slab of the Mongol-Okhotsk Ocean (Donskaya et al., 2013). This conclusion could be further supported by a series of tectono-magmatic discrimination diagrams in which most of the mafic rocks in the rifts plot in the volcanic arc fields (Fig. 7). The A-type granitoids and felsic volcanics in these Permian-Triassic rifts plot in the A₂ field (Donskaya et al., 2013), similar to those in the rifts of the southern active margin of the Mongol-Okhotsk Ocean (Fig. 8). Moreover, the rifts are distributed parallel to the long axis of the Mongol-Okhotsk suture zone (Fig. 9), which indicates that they document multi-stage, back-arc extensions induced by long-lived subduction of the Mongol-Okhotsk Ocean. The Khangay-Khentey forearc belt near the suture zone of the Mongol-Okhotsk orogenic belt (Bussien et al., 2011), the Permian-Triassic Selenge magmatic arc belt (including Khangay and Khentey calc-alkaline batholith) (e.g., Badarch et al., 2002; Donskaya et al., 2013), and the back-arc extension belt in the hinterland demonstrate that a typical trench-arc-backarc basin system developed on the northern active margin of the Mongol-Okhotsk Ocean.

These records delineate a ~5000-km-long belt of multi-stage, back-arc extensions in the

southwestern segment of the Mongol-Okhotsk orogenic belt (Fig. 9), which indicates that, at least during the Permo-Triassic period, the subduction of the Mongol-Okhotsk Ocean plate probably formed a Western Pacific-type margin rather than an Andean-type margin.

CONCLUSIONS

The Late Permian Monhhan ophiolite is the first ophiolite discovered within the southern active margin of the Mongol-Okhotsk orogenic belt rather than in the suture zone. Field, geochemistry, and geochronology evidence indicate that this ophiolite and associated sandstone represent a relict back-arc basin. The contemporaneous S-type granitic dikes intruding the ophiolite likely formed through partial melting of metasediments as a result of magma underplating during back-arc extension.

Based on a review of geochronological and geochemical data, we suggest that the Permian-Triassic rift zones around the Mongol-Okhotsk orogenic belt document multi-stage, back-arc extensions induced by long-lived subduction of the Mongol-Okhotsk Ocean. Combining our discovery, we argue that there is a back-arc extension belt extending >5000 km in the southwestern segment of the Mongol-Okhotsk orogenic belt, which indicates a probable Western Pacific-type active margin during the Permo-Triassic period rather than an Andean-type margin as previously thought.

ACKNOWLEDGMENTS

We are grateful to Chenghao Liu and Shuangrong Zhang for supporting the analytical experiments. We

thank Mihai N. Ducea for handling the manuscript and Munkhtsengel Baatar and Chimedseren Anaad for their support during our field investigations in Mongolia. This work was financially supported by the Strategic Priority Research Program of the Chinese Academy of Sciences (grant no. XDB 41000000) and the National Natural Science Foundation of China (grant nos. 42272262 and 42172241).

REFERENCES CITED

- Badarch, G., Cunningham, W.D., and Windley, B.F., 2002, A new terrane subdivision for Mongolia: Implications for the Phanerozoic crustal growth of Central Asia: *Journal of Asian Earth Sciences*, v. 21, p. 87–110, [https://doi.org/10.1016/S1367-9120\(02\)00017-2](https://doi.org/10.1016/S1367-9120(02)00017-2).
- Blichert-Toft, J., and Albarède, F., 1997, The Lu-Hf isotope geochemistry of chondrites and the evolution of the mantle-crust system: *Earth and Planetary Science Letters*, v. 148, p. 243–258, [https://doi.org/10.1016/S0012-821X\(97\)00040-X](https://doi.org/10.1016/S0012-821X(97)00040-X).
- Brophy, J.G., 2009, La-SiO₂ and Yb-SiO₂ systematics in mid-ocean ridge magmas: Implications for the origin of oceanic plagiogranite: *Contributions to Mineralogy and Petrology*, v. 158, p. 99–111, <https://doi.org/10.1007/s00410-008-0372-3>.
- Bryan, S.E., and Ernst, R.E., 2008, Revised definition of Large Igneous Provinces (LIPs): *Earth-Science Reviews*, v. 86, p. 175–202, <https://doi.org/10.1016/j.earscirev.2007.08.008>.
- Bussien, D., Gombojav, N., Winkler, W., and Quadt, A., 2011, The Mongol-Okhotsk Belt in Mongolia—an appraisal of the geodynamic development by the study of sandstone provenance and detrital zircons: *Tectonophysics*, v. 510, p. 132–150, <https://doi.org/10.1016/j.tecto.2011.06.024>.
- Capaldi, T.N., Horton, B.K., McKenzie, N.R., Stockli, D.F., and Odulum, M.L., 2017, Sediment provenance in contractional orogens: The detrital zircon record from modern rivers in the Andean fold-thrust belt and foreland basin of western Argentina: *Earth and Planetary Science Letters*, v. 479, p. 83–97, <https://doi.org/10.1016/j.epsl.2017.09.001>.
- Cogné, J.P., Kravchinsky, V.A., Halim, N., and Hankard, F., 2005, Late Jurassic-Early Cretaceous closure of the Mongol-Okhotsk Ocean demonstrated by new Mesozoic palaeomagnetic results from the Trans-Baikal area (SE Siberia): *Geophysical Journal International*, v. 163, no. 2, p. 813–832, <https://doi.org/10.1111/j.1365-246X.2005.02782.x>.

- Cole, R.B., and Stewart, B.W., 2009, Continental margin volcanism at sites of spreading ridge subduction: Examples from southern Alaska and western California: *Tectonophysics*, v. 464, p. 118–136, <https://doi.org/10.1016/j.tecto.2007.12.005>.
- Collins, W.J., and Richards, S.W., 2008, Geodynamic significance of S-type granites in circum-Pacific orogens: *Geology*, v. 36, p. 559–562, <https://doi.org/10.1130/G24658A.1>.
- Condie, K.C., 2005, High field strength element ratios in Archean basalts: A window to evolving sources of mantle plumes?: *Lithos*, v. 79, no. 3–4, p. 491–504, <https://doi.org/10.1016/j.lithos.2004.09.014>.
- Dan, W., Li, X.H., Wang, Q., Wang, X.C., and Liu, Y., 2014, Neoproterozoic S-type granites in the Alxa Block, westernmost North China and tectonic implications: In situ zircon UPb-Hf-O isotopic and geochemical constraints: *American Journal of Science*, v. 314, p. 110–153, <https://doi.org/10.2475/01.2014.04>.
- Dilek, Y., and Furnes, H., 2011, Ophiolite genesis and global tectonics: Geochemical and tectonic fingerprinting of ancient oceanic lithosphere: *Geological Society of America Bulletin*, v. 123, p. 387–411, <https://doi.org/10.1130/B30446.1>.
- Dilek, Y., and Sandvol, E., 2009, Seismic structure, crustal architecture and tectonic evolution of the Anatolian-African plate boundary and the Cenozoic orogenic belts in the Eastern Mediterranean region, in Murphy, J.B., Keppe, J.D., and Hynes, A.J., eds., *Ancient Orogenes and Modern Analogues*: London, Geological Society, London Special Publication 327, p. 127–160, <https://doi.org/10.1144/SP327.8>.
- Donskaya, T.V., Gladkochub, D.P., Mazukabzov, A.M., and Ivanov, A.V., 2013, Late Paleozoic–Mesozoic subduction-related magmatism at the southern margin of the Siberian continent and the 150 million-year history of the Mongol-Okhotsk Ocean: *Journal of Asian Earth Sciences*, v. 62, p. 79–97, <https://doi.org/10.1016/j.jseas.2012.07.023>.
- Dostal, J., Owen, J.V., Shellnutt, J.G., Keppe, J.D., Gerel, O., and Corney, R., 2015, Petrogenesis of the Triassic Bayan-Ulan alkaline granitic pluton in the North Gobi rift of central Mongolia: Implications for the evolution of early Mesozoic granitoid magmatism in the Central Asian Orogenic Belt: *Journal of Asian Earth Sciences*, v. 109, p. 50–62, <https://doi.org/10.1016/j.jseas.2015.04.021>.
- Eby, G.N., 1990, The A-type granitoids: A review of their occurrence and chemical characteristics and speculations on their petrogenesis: *Lithos*, v. 26, p. 115–134, [https://doi.org/10.1016/0024-4937\(90\)90043-Z](https://doi.org/10.1016/0024-4937(90)90043-Z).
- Eby, G.N., 1992, Chemical subdivision of the A-type granitoids: Petrogenetic and tectonic implications: *Geology*, v. 20, p. 641–644, [https://doi.org/10.1130/0091-7613\(1992\)020<0641:CSOTAT>2.3.CO;2](https://doi.org/10.1130/0091-7613(1992)020<0641:CSOTAT>2.3.CO;2).
- Furnes, H., and Dilek, Y., 2017, Geochemical characterization and petrogenesis of intermediate to silicic rocks in ophiolites: A global synthesis: *Earth-Science Reviews*, v. 166, p. 1–37, <https://doi.org/10.1016/j.earscirev.2017.01.001>.
- Ganbat, A., Tsujimori, T., Miao, L.C., and Safonova, I., Pastor-Gal'an, D., Anaad, C., Baatar, M., Aoki, S., Aoki, K., and Savinskiy, I., 2021, Late Paleozoic–early Mesozoic granitoids in the Khangay-Khentey basin, Central Mongolia: Implication for the tectonic evolution of the Mongol-Okhotsk Ocean margin: *Lithos*, v. 404–405, <https://doi.org/10.1016/j.lithos.2021.106455>.
- Gao, L.E., Zeng, L.S., and Asimow, P.D., 2017, Contrasting geochemical signatures of fluid-absent versus fluid-fluxed melting of muscovite in metasedimentary sources: The Himalayan leucogranites: *Geology*, v. 45, p. 39–42, <https://doi.org/10.1130/G38336.1>.
- Gladkochub, D.P., Donskaya, T.V., Wingate, M.T.D., Poller, U., Kröner, A., Fedorovsky, V.S., Mazukabzov, A.M., Todt, W., and Pisarevsky, S.A., 2008, Petrology, geochronology, and tectonic implications of c. 500 Ma metamorphic and igneous rocks along the northern margin of the Central Asian Orogen (Olkhon terrane, Lake Baikal, Siberia): *Journal of the Geological Society*, v. 165, p. 235–246, <https://doi.org/10.1144/0016-76492006-125>.
- Gribble, R.F., Stern, R.J., Newman, S., Bloomer, S.H., and O'Hearn, T., 1998, Chemical and isotopic composition of lavas from the northern Mariana trough: Implications for magma genesis in back-arc basins: *Journal of Petrology*, v. 39, no. 1, p. 125–154, <https://doi.org/10.1093/petroj/39.1.125>.
- Griffin, W.L., Pearson, N.J., Belousova, E., Jackson, S.E., van Achterbergh, E., O'Reilly, S.Y., and Shee, S.R., 2000, The Hf isotope composition of cratonic mantle: LAM-MC-ICPMS analysis of zircon megacrysts in kimberlites: *Geochimica et Cosmochimica Acta*, v. 64, p. 133–147, [https://doi.org/10.1016/S0016-7037\(99\)00343-9](https://doi.org/10.1016/S0016-7037(99)00343-9).
- Griffin, W.L., Belousova, E.A., Shee, S.R., Pearson, N.J., and O'Reilly, S.Y., 2004, Archean crustal evolution in the northern Yilgarn Craton: U-Pb and Hf-isotope evidence from detrital zircons: *Precambrian Research*, v. 131, p. 231–282, <https://doi.org/10.1016/j.precamres.2003.12.011>.
- Hopkinson, T.N., Harris, N.B.W., Warren, C.J., Spencer, C.J., Roberts, N.M.W., Horstwood, M.S.A., Parrish, R.R., and EIMF, 2017, The identification and significance of pure sediment-derived granites: *Earth and Planetary Science Letters*, v. 467, p. 57–63, <https://doi.org/10.1016/j.epsl.2017.03.018>.
- Izokh, A.E., Vishnevskii, A.V., Polyakov, G.V., and Shelepaev, R.A., 2011, Age of picrite and picrodolerite magmatism in western Mongolia: *Russian Geology and Geophysics*, v. 52, p. 7–23, <https://doi.org/10.1016/j.rgg.2010.12.002>.
- Jackson, S.E., Pearson, N.J., Griffin, W.L., and Belousova, E.A., 2004, The application of laser ablation-inductively coupled plasma-mass spectrometry to in situ U-Pb zircon geochronology: *Chemical Geology*, v. 211, p. 47–69, <https://doi.org/10.1016/j.chemgeo.2004.06.017>.
- Jahn, B.M., Litvinovsky, B.A., Zanvilevich, A.N., and Reichow, M., 2009, Peralkaline granitoid magmatism in the Mongolian–Transbaikalian Belt: Evolution, petrogenesis and tectonic significance: *Lithos*, v. 113, p. 521–539, <https://doi.org/10.1016/j.lithos.2009.06.015>.
- Jamyangdorj, U., Tungalag, F., and Boishenko, A.F., 1990, Geological map of the central and eastern Mongolia: Ulaanbaatar, Mongolia, Institute of Geological Research Regional Geological Sector, Ministry of Heavy Industries, scale 1:500,000.
- Kearey, P., Klepeis, K.A., and Vine, F.J., 2009, *Global Tectonics* (3rd ed.): Oxford, John Wiley and Sons, 482 p.
- Kelty, T.K., Yin, A., Dash, B., Gehrels, G.E., and Ribeiro, A.E., 2008, Detrital-zircon geochronology of Paleozoic sedimentary rocks in the Hangay–Henty basin, north-central Mongolia: Implications for the tectonic evolution of the Mongol-Okhotsk Ocean in central Asia: *Tectonophysics*, v. 451, p. 290–311, <https://doi.org/10.1016/j.tecto.2007.11.052>.
- Koepke, J., Berndt, J., Feig, S.T., and Holtz, F., 2007, The formation of SiO₂-rich melts within the deep oceanic crust by hydrous partial melting of gabbros: Contributions to Mineralogy and Petrology, v. 153, p. 67–84, <https://doi.org/10.1007/s00410-006-0135-y>.
- Kovalenko, V.I., Yarmolyuk, V.V., Budnikov, S.V., Sal'nikova, E.B., Kovach, V.P., Kotov, A.B., Ponomarchuk, V.A., Kozlov, V.D., and Vladychkin, N.V., 2003, Sources of igneous rocks and genesis of the early Mesozoic tectonomagmatic area of the Mongolia–Transbaikalia magmatic region: 1. Geology and isotope geochronology: *Petrology*, v. 11, no. 2, p. 147–160.
- Kozlovska, A.M., Yarmolyuk, V.V., Sal'mikova, E.B., Travin, A.V., Kotov, A.B., Plotkina, J.V., Kudryashova, E.A., and Savatenkov, V.M., 2015, Late Paleozoic anorogenic magmatism of the Gobi Altai (SW Mongolia): Tectonic position, geochronology and correlation with igneous activity of the Central Asian Orogenic Belt: *Journal of Asian Earth Sciences*, v. 113, p. 524–541, <https://doi.org/10.1016/j.jseas.2015.01.013>.
- Kuzmin, M.I., Yarmolyuk, V.V., and Kravchinsky, V.A., 2010, Phanerozoic hot spot traces and paleogeographic reconstructions of the Siberian continent based on interaction with the African large low shear velocity province: *Earth-Science Reviews*, v. 102, p. 29–59, <https://doi.org/10.1016/j.earscirev.2010.06.004>.
- Li, P., Sun, M., Naransetseg, T., Jourdan, F., Hu, W., and Yuan, C., 2022, First structural observation around the hinge of the Mongolian Orocline (Central Asia): Implications for the geodynamics of oroclinal bending and the evolution of the Mongol-Okhotsk Ocean: *Geological Society of America Bulletin*, v. 134, no. 7–8, p. 1994–2006, <https://doi.org/10.1130/B36200.1>.
- Li, Y., Xu, W.L., Wang, F., Pei, F.P., Tang, J., and Zhao, S., 2017, Triassic volcanism along the eastern margin of the Xing'an Massif, NE China: Constraints on the spatial-temporal extent of the Mongol-Okhotsk tectonic regime: *Gondwana Research*, v. 48, p. 205–223, <https://doi.org/10.1016/j.gr.2017.05.002>.
- Li, Y., Xu, W.L., Tang, J., Pei, F.P., Wang, F., and Sun, C.Y., 2018, Geochronology and geochemistry of Mesozoic intrusive rocks in the Xing'an Massif of NE China: Implications for the evolution and spatial extent of the Mongol-Okhotsk tectonic regime: *Lithos*, v. 304–307, p. 57–73, <https://doi.org/10.1016/j.lithos.2018.02.001>.
- Li, Z.X., Li, X.H., Chung, S.L., Lo, C.H., Xu, X., and Li, W.X., 2012, Magmatic switch-on and switch-off along the South China continental margin since the Permian: Transition from an Andean-type to a Western Pacific-type plate boundary: *Tectonophysics*, v. 532–535, p. 271–290, <https://doi.org/10.1016/j.tecto.2012.02.011>.
- Liu, H., Li, Y., He, H., Huangfu, P., and Liu, Y., 2018, Two-phase southward subduction of the Mongol-Okhotsk oceanic plate constrained by Permian–Jurassic granitoids in the Erguna and Xing'an massifs (NE China): *Lithos*, v. 304–307, p. 347–361, <https://doi.org/10.1016/j.lithos.2018.01.016>.
- Ludwig, K.R., 2003, User's Manual for a Geochronological Toolkit for Microsoft Excel (Isoplots/Ex Version 3.0): Berkeley Geochronology Center Special Publication 4, p. 1–71.
- Lytwyn, J., Lockhart, S., Casey, J., and Kusky, T., 2000, Geochemistry of near-trench intrusives associated with ridge subduction, Seldovia Quadrangle, southern Alaska: *Journal of Geophysical Research: Solid Earth*, v. 105, p. 27,957–27,978, <https://doi.org/10.1029/2000JB900294>.
- Mazukabzov, A.M., Donskaya, T.V., Gladkochub, D.P., and Paderin, I.P., 2010, The late Paleozoic geodynamics of the west Transbaikalian segment of the central Asian fold belt: *Russian Geology and Geophysics*, v. 51, p. 482–491, <https://doi.org/10.1016/j.rgg.2010.04.008>.
- Metelkin, D.V., Gordienko, I.V., and Klimuk, V.S., 2007, Paleomagnetism of Upper Jurassic basalts from Transbaikalia: New data on the time of closure of the Mongol-Okhotsk Ocean and Mesozoic intraplate tectonics of Central Asia: *Russian Geology and Geophysics*, v. 48, p. 825–834, <https://doi.org/10.1016/j.rgg.2007.09.004>.
- Miao, L., Baatar, M., Zhang, F., Anaad, C., Zhu, M., and Yang, S., 2016, Cambrian Kherlen ophiolite in northeastern Mongolia and its tectonic implications: SHRIMP zircon dating and geochemical constraints: *Lithos*, v. 261, p. 128–143, <https://doi.org/10.1016/j.lithos.2015.12.012>.
- Narantsetseg, T., Orolmaa, D., Yuan, C., Wang, T., Guo, L., Tong, Y., Wang, X., Enkh-Orszhikh, O., Oyunchimeg, T.U., Delgerzaya, P., and Enkhdalai, B., 2019, Early–Middle Paleozoic volcanic rocks from the Ereendavaa terrane (Tsarigii gol area, NE Mongolia) with implications for tectonic evolution of the Kherlen massif: *Journal of Asian Earth Sciences*, v. 175, p. 138–157, <https://doi.org/10.1016/j.jseas.2018.12.008>.
- Parfenov, L.M., Popko, L.I., and Tomurtogoo, O., 2001, Problems of tectonics of the Mongol-Okhotsk orogenic belt: *Geology of the Pacific Ocean*, v. 16, p. 797–830.
- Paton, C., Woodhead, J.D., Hellstrom, J.C., Hergt, J.M., Greig, A., and Maas, R., 2010, Improved laser ablation U-Pb zircon geochronology through robust downhole fractionation correction: *Geochemistry, Geophysics, Geosystems*, v. 11, Q0AA06.
- Pearce, J.A., 2008, Geochemical fingerprinting of oceanic basalts with applications to ophiolite classification and the search for Archean oceanic crust: *Lithos*, v. 100, p. 14–48, <https://doi.org/10.1016/j.lithos.2007.06.016>.
- Pearce, J.A., Harris, N.B.W., and Tindle, A.G., 1984, Trace element discrimination diagrams for the tectonic interpretation of granitic rocks: *Journal of Petrology*, v. 25, p. 956–983, <https://doi.org/10.1093/petrology/25.4.956>.

- Plank, T., 2005, Constraints from thorium/lanthanum on sediment recycling at subduction zones and the evolution of the continents: *Journal of Petrology*, v. 46, no. 5, p. 921–944, <https://doi.org/10.1093/petrology/egi005>.
- Ramos, V.A., and Folguera, A., 2009, Andean flat-slab subduction through time, in Murphy, J.B., ed., *Ancient Orogenes and Modern Analogues*: Geological Society, London, Special Publication 327, p. 31–54.
- Reichow, M.K., Litvinovsky, B.A., Parrish, R.R., and Saunders, A.D., 2010, Multi-stage emplacement of alkaline and peralkaline syenite–granite suites in the Mongolian–Transbaikalian Belt, Russia: Evidence from U–Pb geochronology and whole rock geochemistry: *Chemical Geology*, v. 273, p. 120–135, <https://doi.org/10.1016/j.chemgeo.2010.02.017>.
- Ren, Q., Zhang, S., Wu, Y., Yang, T., Gao, Y., Turbold, S., Zhao, H., Wu, H., Li, H., and Fu, H., 2018, New Late Jurassic to Early Cretaceous Paleomagnetic Results From North China and Southern Mongolia and Their Implications for the Evolution of the Mongol–Okhotsk Suture: *Journal of Geophysical Research: Solid Earth*, v. 123, p. 10370–10398, <https://doi.org/10.1029/2018JB016703>.
- Rubatto, D., 2002, Zircon trace element geochemistry: partitioning with garnet and the link between U–Pb ages and metamorphism: *Chemical Geology*, v. 184, no. 1–2, p. 123–138, [https://doi.org/10.1016/S0009-2541\(01\)00355-2](https://doi.org/10.1016/S0009-2541(01)00355-2).
- Ryttsk, E.Y., Kovach, V.P., Makeev, A.F., Bogomolov, E.S., and Rizvanova, N.G., 2009, The eastern boundary of the Baikal collisional belt: Geological, geochronological, and Nd isotopic evidence: *Geotectonics*, v. 43, no. 4, p. 264–273, <https://doi.org/10.1134/S0016852109040025>.
- Saccani, E., 2015, A new method of discriminating different types of post-Archean ophiolitic basalts and their tectonic significance using Th–Nb and Ce–Dy–Yb systematics: *Geoscience Frontiers*, v. 6, p. 481–501, <https://doi.org/10.1016/j.gsf.2014.03.006>.
- Saunders, A.D., and Tarney, J., 1984, Geochemical characteristics of basaltic volcanism within back-arc basins, in Kokelaar, B.P., and Howells, M.F., eds., *Marginal Basin Geology: Volcanic and Associated Sedimentary and Tectonic Processes in Modern and Ancient Marginal Basins*: Geological Society, London, Special Publication 16, p. 59–76, <https://doi.org/10.1144/GSL.SP.1984.016.01.05>.
- Sengör, A.M.C., and Natal' in, B.A., 1996, *Palaeotectonics of Asia: Fragments of a synthesis*, in Yin, A., and Harrison, T.M., eds., *The Tectonic Evolution of Asia*: Cambridge, UK, Cambridge University Press, p. 486–640.
- Shinjo, R., Chung, S.L., Kato, Y., and Kimura, M., 1999, Geochemical and Sr–Nd isotopic characteristics of volcanic rocks from the Okinawa Trough and Ryukyu Arc: Implications for the evolution of a young, intracontinental back arc basin: *Journal of Geophysical Research: Solid Earth*, v. 104, p. 10,591–10,608, <https://doi.org/10.1029/1999JB900040>.
- Sláma, J., Kosler, J., Condon, D.J., Crowley, J.L., Gerdes, A., Hanchar, J.M., Horstwood, M.S.A., Morris, G.A., Nasdala, L., Norberg, N., Schaltegger, U., Schoene, B., Tubrett, M.N., and Whitehouse, M.J., 2008, Plesovice zircon—A new natural reference material for U–Pb and Hf isotopic microanalysis: *Chemical Geology*, v. 249, p. 1–35, <https://doi.org/10.1016/j.chemgeo.2007.11.005>.
- Sorokin, A.A., Zaika, V.A., Kovach, V.P., Kotov, A.B., Xu, W.L., and Yang, H., 2020, Timing of closure of the eastern Mongol–Okhotsk Ocean: Constraints from U–Pb and Hf isotopic data of detrital zircons from metasediments along the Dzhagdy Transect: *Gondwana Research*, v. 81, p. 58–78, <https://doi.org/10.1016/j.gr.2019.11.009>.
- Stern, R.J., 2002, Subduction zones: *Reviews of Geophysics*, v. 40, no. 4, p. 3–1–3–38, <https://doi.org/10.1029/2001RG000108>.
- Stern, R.J., 2010, The anatomy and ontogeny of modern intra-oceanic arc systems, in Kusky, T.M., Zhai, M.G., Xiao, W., eds., *The Evolving Continents: Understanding Processes of Continental Growth*: Geological Society, London, Special Publication 338, p. 7–34, <https://doi.org/10.1144/SP338.2>.
- Sun, D.Y., Gou, J., Wang, T.H., Ren, Y.S., Liu, Y.J., Guo, H.Y., Liu, X.M., and Hu, Z.C., 2013, Geochronologi-
- cal and geochemical constraints on the Erguna massif basement, NE China—subduction history of the Mongol–Okhotsk oceanic crust: *International Geology Review*, v. 55, no. 14, p. 1801–1816, <https://doi.org/10.1080/00206814.2013.804664>.
- Sun, S.S., and McDonough, W.F., 1989, Chemical and isotopic systematics of oceanic basalts: implications for mantle composition and processes, in Saunders, A.D., and Norry, M.J., eds., *Magmatism in the Ocean Basins*: Geological Society Special Publication 42, pp. 313–345, <https://doi.org/10.1144/GSL.SP.1989.042.01.19>.
- Tang, J., Xu, W.L., Wang, F., Zhao, S., and Wang, W., 2016, Early Mesozoic southward subduction history of the Mongol–Okhotsk oceanic plate: Evidence from geochronology and geochemistry of early Mesozoic intrusive rocks in the Erguna Massif, NE China: *Gondwana Research*, v. 31, p. 218–240, <https://doi.org/10.1016/j.gr.2014.12.010>.
- Taylor, S.R., and McLennan, S., 1995, The geochemical evolution of the continental crust: *Review of Geophysics*, v. 33, p. 241–265, <https://doi.org/10.1029/95RG00262>.
- Tomurtogoo, O., Windley, B.F., Kroner, A., Badarch, G., and Liu, D.Y., 2005, Zircon age and occurrence of the Adaatsag ophiolite and Muron shear zone, central Mongolia: Constraints on the evolution of the Mongol–Okhotsk Ocean, suture and orogeny: *Journal of the Geological Society*, v. 162, p. 125–134, <https://doi.org/10.1144/0016-7649-03-146>.
- Uyeda, S., 1982, Subduction zones: An introduction to comparative subductology: *Tectonophysics*, v. 81, p. 133–159, [https://doi.org/10.1016/0040-1951\(82\)90126-3](https://doi.org/10.1016/0040-1951(82)90126-3).
- Van der Voo, R., van Hinsbergen, D.J., Domeier, M., Spakman, W., and Torsvik, T.H., 2015, Latest Jurassic–earliest Cretaceous closure of the Mongol–Okhotsk Ocean: A paleomagnetic and seismological-tomographic analysis, in Anderson, T.H., Didenko, A.N., Johnson, C.L., Khanchuk, A.I., and MacDonald, A.H., Jr., eds., *Late Jurassic Margin of Laurasia—A Record of Faulting Accommodating Plate Rotation*: Geological Society of America Special Paper 513, p. 589–606, [https://doi.org/10.1130/2015.2513\(19\)](https://doi.org/10.1130/2015.2513(19)).
- Vorontsov, A.A., Yarmolyuk, V.V., Dril, S.I., Tatarnikov, S.A., Sandimirova, G.P., Yarmolyuk, V.V., and Lykhin, D.A., 2007, Magmatic sources and geodynamics of the early Mesozoic Northern Mongolia–Western Transbaikalia rift zone: *Petrology*, v. 15, no. 1, p. 35–57, <https://doi.org/10.1134/S0869591107010031>.
- Wilhem, C., Windley, B.F., and Stampfli, G.M., 2012, The Altaiids of Central Asia: A tectonic and evolutionary innovative review: *Earth-Science Reviews*, v. 113, p. 303–341, <https://doi.org/10.1016/j.earscirev.2012.04.001>.
- Windley, B.F., Alexeev, D., Xiao, W., Kroner, A., and Badarch, G., 2007, Tectonic models for accretion of the Central Asian Orogenic Belt: *Journal of the Geological Society*, v. 164, p. 31–47, <https://doi.org/10.1144/0016-7649-2006-022>.
- Wood, D.A., 1980, The application of a Th–Hf–Ta diagram to problems of tectonomagmatic classification and to establishing the nature of crustal contamination of basaltic lavas of the British Tertiary Volcanic Province: *Earth and Planetary Science Letters*, v. 50, no. 1, p. 11–30, [https://doi.org/10.1016/0012-821X\(80\)90116-8](https://doi.org/10.1016/0012-821X(80)90116-8).
- Wu, F.Y., Yang, Y.H., Xie, L.W., Yang, J.H., and Xu, P., 2006, Hf isotopic compositions of the standard zircons and baddeleyites used in U–Pb geochronology: *Chemical Geology*, v. 234, p. 105–126, <https://doi.org/10.1016/j.chemgeo.2006.05.003>.
- Xiao, W., Windley, B.F., Sun, S., Li, J., Huang, B., Han, C., Yuan, C., Sun, M., and Chen, H., 2015, A tale of amalgamation of three Permo-Triassic collage systems in Central Asia: Oroclines, sutures, and terminal accretion: *Annual Review of Earth and Planetary Sciences*, v. 43, p. 477–507, <https://doi.org/10.1146/annurev-earth-060614-105254>.
- Xu, J., Xia, X.P., Wang, Q., Spencer, C.J., Lai, C.K., Ma, J.L., Zhang, L., Cui, Z.X., Zhang, W.F., and Zhang, Y.Q., 2021, Pure sediment-derived granites in a subduction zone: *Geological Society of America Bulletin*, v. 134, no. 3–4, p. 599–615.
- Xu, W.L., Pei, F.P., Wang, F., Meng, E., Ji, W.Q., Yang, D.B., and Wang, W., 2013, Spatial–temporal relationships of Mesozoic volcanic rocks in NE China: Constraints on tectonic overprinting and transformations between multiple tectonic regimes: *Journal of Asian Earth Sciences*, v. 74, p. 167–193, <https://doi.org/10.1016/j.jseaes.2013.04.003>.
- Yang, J., Wang, J.R., Zhang, Q., Chen, W.F., Pan, Z.J., Jiao, S.T., and Wang, S.H., 2016, Back-arc basin basalt (BABB) data mining: Comparison with MORB and IAB [in Chinese with English abstract]: *Diqu Kuixue Jinzhan*, v. 31, no. 1, p. 66–77.
- Yarmolyuk, V.V., Kovalenko, V.I., Salnikova, E.B., Budnikov, S.V., Kovach, V.P., Kotov, A.B., and Ponomarchuk, V.A., 2002, Tectono-magmatic zoning, magma sources, and geodynamic of the Early Mesozoic Mongolo–Transbaikalian magmatic area: *Geotectonics*, v. 36, p. 293–311.
- Yarmolyuk, V.V., Kovalenko, V.I., Kozakov, I.K., Sal'nikova, E.B., Bibikova, E.V., Kovach, V.P., Kozlovsky, A.M., Kotov, A.B., Lebedev, V.I., Eenjin, G., and Fugzan, M.M., 2008, The age of the Khangai batholith and the problem of batholith formation in Central Asia: *Doklady Earth Sciences*, v. 423, p. 1223–1228, <https://doi.org/10.1134/S1028334X0800096>.
- Yarmolyuk, V.V., Kuzmin, M.I., and Kozlovsky, A.M., 2013, Late Paleozoic–Early Mesozoic within-plate magmatism in North Asia: traps, rifts, giant batholiths, and the geodynamics of their origin: *Petrology*, v. 21, no. 2, p. 101–126, <https://doi.org/10.1134/S0869591113010062>.
- Yarmolyuk, V.V., Kuzmin, M.I., and Ernst, R.E., 2014, Intraplate geodynamics and magmatism in the evolution of the Central Asian Orogenic Belt: *Journal of Asian Earth Sciences*, v. 93, p. 158–179, <https://doi.org/10.1016/j.jseaes.2014.07.004>.
- Yi, Z., and Meert, J.G., 2020, A closure of the Mongol–Okhotsk Ocean by the Middle Jurassic: Reconciliation of paleomagnetic and geological evidence: *Geophysical Research Letters*, v. 47, <https://doi.org/10.1029/2020GL088235>.
- Zhang, F.Q., Dilek, Y., Chen, H.L., Yang, S.F., and Meng, Q.A., 2017, Late Cretaceous tectonic switch from a Western Pacific- to an Andean-type continental margin evolution in East Asia, and a foreland basin development in NE China: *Terra Nova*, v. 29, p. 335–342, <https://doi.org/10.1111/ter.12286>.
- Zhao, P., Xu, B., and Jahn, B.M., 2017, The Mongol–Okhotsk Ocean subduction-related Permian peraluminous granites in northeastern Mongolia: Constraints from zircon U–Pb ages, whole-rock elemental and Sr–Nd–Hf isotopic compositions: *Journal of Asian Earth Sciences*, v. 144, p. 225–242, <https://doi.org/10.1016/j.jseaes.2017.03.022>.
- Zheng, Y.F., Chen, Y.X., Dai, L.Q., and Zhao, Z.F., 2015, Developing plate tectonics theory from oceanic subduction zones to collisional orogens: *Science China Earth Sciences*, v. 58, p. 1045–1069, <https://doi.org/10.1007/s11430-015-5097-3>.
- Zhu, M.S., Zhang, F.Q., Miao, L.C., Baatar, M., Anaad, C., Yang, S.H., and Li, X.B., 2016, Geochronology and geochemistry of the Triassic bimodal volcanic rocks and coeval A-type granites of the Olzii area, Middle Mongolia: Implications for the tectonic evolution of Mongol–Okhotsk Ocean: *Journal of Asian Earth Sciences*, v. 122, p. 41–57, <https://doi.org/10.1016/j.jseaes.2016.03.001>.
- Zhu, M.S., Zhang, F.Q., Miao, L.C., Baatar, M., Anaad, C., Yang, S.H., and Li, X.B., 2018, The Late Carboniferous Khuhu Davaa ophiolite in northeastern Mongolia: Implications for the tectonic evolution of the Mongol–Okhotsk Ocean: *Geological Journal*, v. 53, p. 1263–1278, <https://doi.org/10.1002/gj.2955>.
- Zorin, Y.A., 1999, Geodynamics of the western part of the Mongolia–Okhotsk collisional belt, Trans-Baikal region (Russia) and Mongolia: *Tectonophysics*, v. 306, p. 33–56, [https://doi.org/10.1016/S0040-1951\(99\)00042-6](https://doi.org/10.1016/S0040-1951(99)00042-6).

SCIENCE EDITOR: MIHAI DUCEA

ASSOCIATE EDITOR: VERONICA OLIVEROS CLAVIJO

MANUSCRIPT RECEIVED 19 JUNE 2022

REVISED MANUSCRIPT RECEIVED 6 SEPTEMBER 2022

MANUSCRIPT ACCEPTED 30 OCTOBER 2022

Printed in the USA